Pergamon

Computers Math. Applic. Vol. 35, No. 1/2, pp. 15–28, 1998

0898-1221/98 $19.00 + 0.00

PII: S0898-1221(97)00255-1

A Rarefied Gas Flow Induced by a Temperature Field: Numerical Analysis of the Flow between Two Coaxial Elliptic Cylinders with Different Uniform Temperatures

K. AOKI, Y. SONE AND Y. WANIGUCHI
Department of Aeronautics and Astronautics, Graduate School of Engineering
Kyoto University, Kyoto 606-01, Japan

Abstract—A steady flow of a rarefied gas induced by a temperature field is investigated, on the basis of kinetic theory, for the case where the temperature of each boundary is uniform (i.e., where the flow caused by the nonuniformity of the boundary temperature, such as the thermal transpiration flow, vanishes). More specifically, a rarefied gas confined in the gap between two coaxial elliptic cylinders at rest with different uniform temperatures is considered, and the steady gas flow induced in the gap is analyzed numerically by the direct simulation Monte Carlo method for a wide range of the Knudsen number. The flow patterns, together with the density and temperature fields, are obtained, and the features of the flow are clarified.

Keywords—Rarefied gas flows, Kinetic theory of gases, Boltzmann equation, Direct simulation Monte Carlo method, Thermal creep flow.

1. INTRODUCTION

In a rarefied gas, in contrast to the Navier-Stokes gas, a steady flow can be induced by a steady temperature field even when there is no external force. For small Knudsen numbers, the features of such flows have been clarified on the basis of the asymptotic theory [1–5], a general theory describing the steady behavior of the gas at small Knudsen numbers, derived systematically from the Boltzmann equation. According to the results, in addition to the well-known thermal creep flow [6–8] induced along a boundary with a nonuniform temperature, the thermal stress slip flow (TSS flow for short) [2,9,10] and the nonlinear thermal stress flow (NTS flow) [4,5,11] are caused in the gas. The TSS flow is induced over a boundary along which the temperature gradient of the gas normal to the boundary is not uniform, and the NTS flow occurs in the gas where the distance between isothermal surfaces varies along them. Thus, both flows can be induced in the case where the thermal creep flow vanishes, i.e., where the temperature of each boundary is uniform. The NTS flow, which is of the first order of the Knudsen number, is negligible when the temperature variation in the system is small. On the other hand, the TSS flow occurs even when the temperature variation is small, though it is of the second order of the Knudsen number. Thus, the TSS flow is important in a small system as in micromachines, since the large temperature difference in a small distance hardly occurs.

The above flows for small Knudsen numbers are classified by the local temperature field. In contrast, for nonsmall or intermediate Knudsen numbers, the features of the induced flow are not characterized by the local temperature but are directly affected by the overall properties, i.e., the configuration of the system. In this situation, therefore, systems with various configurations should be investigated in order to clarify the features of the flow. However, it should be noted

that, if the temperature of a boundary is not uniform, a flow usually occurs along it. The thermal transpiration flow [12] and the thermophoresis of an aerosol particle [13] are typical examples of the flow. This flow makes it difficult to observe other types of flow caused by the direct effect of the configuration of the system. Therefore, for the purpose of clarifying the properties of the latter types of flow, we should investigate systems where the temperature of each boundary is uniform.

In the present study, therefore, we consider such a system, i.e., a system where a uniformly cooled (or heated) body is placed in a rarefied gas confined in a closed vessel with a uniform temperature. More specifically, we consider a rarefied gas confined in the gap between two coaxial elliptic cylinders with different uniform temperatures and investigate the steady gas flow induced in the gap on the basis of kinetic theory. The analysis is carried out numerically by the direct simulation Monte Carlo (DSMC) method [14,15], and the behavior of the gas is clarified for a wide range of the Knudsen number.

Now we should mention our previous works closely related to the present problem. In [16], a similar problem (a gas between noncoaxial circular cylinders) was investigated, in the case where the temperature difference between the body and the vessel is small (linearized problem), by an accurate finite-difference analysis of the linearized Boltzmann-Krook-Welander (BKW) equation, and the behavior of the flow was clarified for the whole range of the Knudsen number. The case with a large temperature difference (nonlinear problem) was studied in [17], where a body with sharp edges (flat plate) was considered with special interest in the effect of the edges on the flow. The behavior of the gas was analyzed for a wide range of the Knudsen number by the DSMC method, and it was shown that a fairly intense flow is induced by the effect of the sharp edges. The relation between these previous results and the flow in the present problem (nonlinear problem with a smooth boundary) will also be discussed.

2. PROBLEM

Let us consider a rarefied gas in the two-dimensional domain between two coaxial elliptic cylinders at rest. Let the surface of the outer cylinder (pipe) be given by $(X_1/a_1)^2 + X_2^2 = L^2$, $(a_1 > 0,\ L > 0)$, and that of the inner cylinder by $(X_1/a_0)^2 + (X_2/b_0)^2 = L^2$, $(0 < a_0 < a_1,\ 0 < b_0 < 1)$, where (X_1, X_2, X_3) is the rectangular space coordinate system with the X_3 axis along the common axis of the cylinders. Further, we assume that the inner cylinder is kept at a uniform temperature T_0 and the outer cylinder is kept at another uniform temperature T_1. (See Figure 1.) We investigate the steady behavior of the gas for a wide range of the Knudsen number on the basis of kinetic theory under the following assumptions.

(i) The gas molecules are hard spheres of a uniform size and undergo complete elastic collisions among themselves.

(ii) The gas molecules make diffuse reflection on the surfaces of the inner and outer cylinders.

We now summarize the additional main notations used in this paper: $\boldsymbol{\xi} = (\xi_1, \xi_2, \xi_3)$ is the molecular velocity, $f(X_1, X_2, \boldsymbol{\xi})$ is the velocity distribution function of the gas molecules, ρ is the density of the gas, $\mathbf{v} = (v_1, v_2, v_3)$ is its flow velocity $(v_3 = 0)$, T is its temperature, ρ_0 is the average density of the gas over the domain, m is the mass of a gas molecule, d_m is its diameter, $l_0 = (\sqrt{2}\pi d_m^2 \rho_0/m)^{-1}$ is the mean free path of the gas molecules in the equilibrium state at rest with density ρ_0 and temperature T_0, $\mathrm{Kn} = l_0/L$ is the Knudsen number, and R is the gas constant per unit mass.

3. BASIC EQUATION AND BOUNDARY CONDITION

The present problem, which is time-independent and spatially two-dimensional, is symmetric with respect to the X_1 and X_2 axes. Therefore, we can analyze the problem only in the first quadrant by imposing the specular reflection condition on the symmetry axes in the gas.

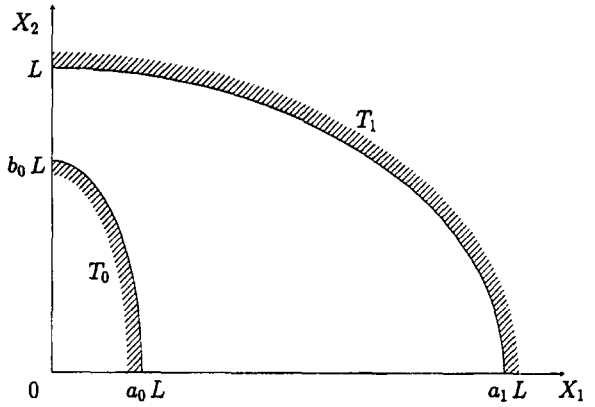

Figure 1. Rarefied gas between two elliptic cylinders (the first quadrant).

The Boltzmann equation in the present situation is written as follows [5,18]:

$$\xi_1 \frac{\partial f}{\partial X_1} + \xi_2 \frac{\partial f}{\partial X_2} = J(f, f), \tag{1}$$

$$J(f, f) = \frac{1}{m} \int (f' f'_* - f f_*) B d\Omega(\boldsymbol{\alpha})\, d\xi_{1*}\, d\xi_{2*}\, d\xi_{3*}, \tag{2}$$

with

$$B = \frac{|(\boldsymbol{\xi}_* - \boldsymbol{\xi}) \cdot \boldsymbol{\alpha}| d_m^2}{2}, \tag{3}$$

$$\begin{aligned} f &= f(X_1, X_2, \boldsymbol{\xi}), & f_* &= f(X_1, X_2, \boldsymbol{\xi}_*), \\ f' &= f(X_1, X_2, \boldsymbol{\xi}'), & f'_* &= f(X_1, X_2, \boldsymbol{\xi}'_*), \\ \boldsymbol{\xi}' &= \boldsymbol{\xi} + [(\boldsymbol{\xi}_* - \boldsymbol{\xi}) \cdot \boldsymbol{\alpha}]\boldsymbol{\alpha}, & \boldsymbol{\xi}'_* &= \boldsymbol{\xi}_* - [(\boldsymbol{\xi}_* - \boldsymbol{\xi}) \cdot \boldsymbol{\alpha}]\boldsymbol{\alpha}, \end{aligned} \tag{4}$$

where $\boldsymbol{\alpha}$ is a unit vector, $d\Omega(\boldsymbol{\alpha})$ is the solid angle element around $\boldsymbol{\alpha}$, $\boldsymbol{\xi}_* = (\xi_{1*}, \xi_{2*}, \xi_{3*})$ is the variable of integration corresponding to $\boldsymbol{\xi}$, and the integration is carried out over the whole space of $\boldsymbol{\alpha}$ and that of $\boldsymbol{\xi}_*$.

The boundary condition on the inner and outer cylinders is given as

$$f = \frac{\rho_w}{(2\pi R T_w)^{3/2}} \exp\left(-\frac{\xi_1^2 + \xi_2^2 + \xi_3^2}{2RT_w}\right), \qquad (\boldsymbol{\xi} \cdot \mathbf{n} > 0), \tag{5}$$

with

$$\rho_w = -\left(\frac{2\pi}{RT_w}\right)^{1/2} \int_{\boldsymbol{\xi} \cdot \mathbf{n} < 0} \boldsymbol{\xi} \cdot \mathbf{n} f\, d\xi_1\, d\xi_2\, d\xi_3, \tag{6}$$

$$T_w = \begin{cases} T_0, & \text{(on the inner cylinder)}, \\ T_1, & \text{(on the outer cylinder)}, \end{cases}$$

where $\mathbf{n}$ is the unit normal vector, pointing into the gas, to the boundary.

The symmetry condition on the X_1 and X_2 axes in the domain of the gas ($a_0 L < X_1 < a_1 L$, $X_2 = 0$ and $X_1 = 0$, $b_0 L < X_2 < L$) is expressed as

$$f(X_1, X_2, \boldsymbol{\xi}) = f(X_1, X_2,\ \boldsymbol{\xi} - 2(\boldsymbol{\xi} \cdot \mathbf{n})\mathbf{n}), \qquad (\boldsymbol{\xi} \cdot \mathbf{n} > 0), \tag{7}$$

where $\mathbf{n} = (0, 1, 0)$ on the X_1 axis and $\mathbf{n} = (1, 0, 0)$ on the X_2 axis.

The macroscopic variables are expressed by the moments of f, e.g.,

$$\begin{aligned} \rho &= \int f\, d\xi_1\, d\xi_2\, d\xi_3, \\ \mathbf{v} &= \frac{1}{\rho} \int \boldsymbol{\xi} f\, d\xi_1\, d\xi_2\, d\xi_3, \\ T &= \left(\frac{1}{3R\rho}\right) \int (\boldsymbol{\xi} - \mathbf{v}) \cdot (\boldsymbol{\xi} - \mathbf{v}) f\, d\xi_1\, d\xi_2\, d\xi_3, \end{aligned} \tag{8}$$

where the range of integration is the whole space of $\boldsymbol{\xi}$.

4. OUTLINE OF NUMERICAL ANALYSIS

We analyze the boundary-value problem (1), (5), and (7) by the standard DSMC method (see [14,15]). The method is basically time-dependent. Thus, we obtain the solution as the long-time limit of the solution of the unsteady problem composed of the time-dependent Boltzmann equation (equation (1) with the time-derivative term $\frac{\partial f}{\partial t}$ (t is the time) added to the left-hand side), the boundary conditions (5) and (7), and an appropriately chosen initial velocity distribution

$$f = f^{(0)}. \tag{9}$$

The outline of the process of DSMC computation is summarized as follows [5].

(i) We divide the gas region in the first quadrant in the X_1X_2 plane into S small cells of unequal size.

(ii) We assign $N_{(\ell)}$ particles to the ℓ^{th} cell ($\ell = 1, 2, \ldots, S$), where $N_{(\ell)}$ is chosen to be proportional to the area of the cell $A_{(\ell)}$ and to the density $\rho^{(0)}_{(\ell)}$ at a representative point in the cell corresponding to the initial velocity distribution (9), i.e.,

$$N_{(\ell)} = \frac{\rho^{(0)}_{(\ell)} A_{(\ell)}}{C_0 m}, \tag{10}$$

with C_0 being a constant that is common to all the cells. The positions of the particles are distributed randomly in the cell, and their velocities are distributed according to the initial velocity distribution (9).

(iii) Let $\mathbf{X}^{(n)}$ and $\boldsymbol{\xi}^{(n)}$ be the position and velocity of the n^{th} particle ($n = 1, 2, \ldots, N$, where $N = \sum_{\ell=1}^{S} N_{(\ell)}$). For a small time step Δt, we change the position of each particle in the X_1X_2 plane as $(X_1^{(n)}, X_2^{(n)}) \to (X_1^{(n)} + \xi_1^{(n)}\Delta t,\ X_2^{(n)} + \xi_2^{(n)}\Delta t)$. The particles that go out from the gas region in this change are cast in the region according to the condition (5) or (7). Here recounting the number of the particles in each cell, we take the new number as $N_{(\ell)}$.

(iv) The collision process of the particles in each cell ($A_{(\ell)}$) is computed independently from other cells as follows. To a pair of the particles with velocities $\boldsymbol{\xi}^{(j)}$ and $\boldsymbol{\xi}^{(k)}$, we assign the following probability $P^{(j,k)}_{(\ell)}$ for their collision:

$$P^{(j,k)}_{(\ell)} = \pi d_m^2 C_0 \left|\boldsymbol{\xi}^{(k)} - \boldsymbol{\xi}^{(j)}\right| \frac{\Delta t}{A_{(\ell)}}. \tag{11}$$

We first choose $M_{(\ell)}$ pairs randomly from the $N_{(\ell)}(N_{(\ell)}-1)/2$ pairs in the cell, where $M_{(\ell)}$ is a number such that

$$\begin{aligned} M_{(\ell)} &\ll \frac{N_{(\ell)}(N_{(\ell)}-1)}{2}, \\ M_{(\ell)} &- \left[\frac{N_{(\ell)}(N_{(\ell)}-1)}{2}\right] \max P^{(j,k)}_{(\ell)} \gg 1. \end{aligned} \tag{12}$$

Then, for each of $M_{(\ell)}$ pairs, we determine whether it collides or not according to the elevated probability for their collision,

$$P^{(j,k)}_{M(\ell)} = \left[\frac{N_{(\ell)}(N_{(\ell)}-1)}{2M_{(\ell)}}\right] P^{(j,k)}_{(\ell)}. \tag{13}$$

The determination of the collision pairs by the above two steps instead of equation (11) is a time-saving procedure, which is efficient and legitimate for small $P^{(j,k)}_{(\ell)}$. For the pairs

that collide, we select a unit vector $\boldsymbol{\alpha}$ assuming that the probability for $\boldsymbol{\alpha}$ lying in the solid-angle element $d\Omega$ is

$$\frac{|(\boldsymbol{\xi}^{(k)} - \boldsymbol{\xi}^{(j)}) \cdot \boldsymbol{\alpha}| d\Omega}{2\pi |\boldsymbol{\xi}^{(k)} - \boldsymbol{\xi}^{(j)}|},$$

and replace their velocities $(\boldsymbol{\xi}^{(j)}, \boldsymbol{\xi}^{(k)})$ by $(\boldsymbol{\xi}^{(j)} + [(\boldsymbol{\xi}^{(k)} - \boldsymbol{\xi}^{(j)}) \cdot \boldsymbol{\alpha}]\boldsymbol{\alpha}, \boldsymbol{\xi}^{(k)} - [(\boldsymbol{\xi}^{(k)} - \boldsymbol{\xi}^{(j)}) \cdot \boldsymbol{\alpha}]\boldsymbol{\alpha})$. The velocities of the pairs that do not collide are left unchanged. With the new velocities $\boldsymbol{\xi}^{(j)}$, we construct the velocity distribution function f at the cell under consideration after time Δt as

$$f = \left(\frac{mC_0}{A_{(\ell)}}\right) \sum_{\text{all } j \text{ in } A_{(\ell)}} \delta\left(\boldsymbol{\xi} - \boldsymbol{\xi}^{(j)}\right), \tag{14}$$

where $\delta(\boldsymbol{\xi})$ is the (three-dimensional) delta function. From equation (8) with equation (14), the density, flow velocity, and temperature of the gas at the cell is expressed as

$$\begin{aligned} \rho &= \frac{mC_0 N_{(\ell)}}{A_{(\ell)}}, \\ \mathbf{v} &= \left(\frac{1}{N_{(\ell)}}\right) \sum_{\text{all } j \text{ in } A_{(\ell)}} \boldsymbol{\xi}^{(j)}, \\ T &= \left(\frac{1}{3RN_{(\ell)}}\right) \sum_{\text{all } j \text{ in } A_{(\ell)}} \left(\boldsymbol{\xi}^{(j)} - \mathbf{v}\right) \cdot \left(\boldsymbol{\xi}^{(j)} - \mathbf{v}\right). \end{aligned} \tag{15}$$

We carry out the above procedure for all the cells.

(v) With the new positions in process (iii) and new velocities in process (iv) of the particles, we go back to process (iii).

We repeat processes (iii)–(v) until the steady state is judged to be established.

The procedure described above, which is a standard method of DSMC (Bird's method), is shown to be mathematically consistent with the Boltzmann equation as well as physically natural [5,19]. That is, in the present problem, the velocity distribution function at arbitrary time t obtained by repeating processes (iii)–(v) converges to the solution of the time-dependent Boltzmann equation subject to boundary conditions (5) and (7) and to initial condition (9) in the limit $N_{(\ell)} \to \infty$ and $D_{(\ell)} \to 0$ in each cell and $\Delta t \to 0$ (with $|\boldsymbol{\xi}^{(j)}|_{\max} \Delta t \lesssim D_{(\ell)}$ in each cell), where $D_{(\ell)}$ is the linear dimension of the cell $A_{(\ell)}$ (thus $A_{(\ell)} \sim D_{(\ell)}^2$ for the cell of a regular shape). The convergence means that any moments of f of the form (14) in each cell become arbitrarily close to the corresponding moments of the solution of the Boltzmann equation (weak convergence) (see [5] for the details).

In the actual computation, where the available number of particles and that of cells are restricted by computing capacity and time, the true steady state is never reached even after a long time, that is, the macroscopic variables as well as the velocity distribution function always show large temporal fluctuations. Therefore, the steady state is judged to be established if, for example, the averages of macroscopic variables at each time step over a certain time interval (consisting of a large number of time steps) are independent of the choice of the interval. We usually compute the average of the fluctuating "steady" solution over a great number of time steps and regard the result as the desired steady solution. This averaging process, however, has not been legitimated so far.

5. RESULTS OF NUMERICAL ANALYSIS

First, the computation for the case with $a_0 = 0.3$, $b_0 = 0.7$, and $a_1 = 1.5$ and with $T_1/T_0 = 5$ is performed for a wide range of the Knudsen number (from relatively small to large one). The behavior of the gas in this range is well represented by the cases shown in Figures 2 and 3. In

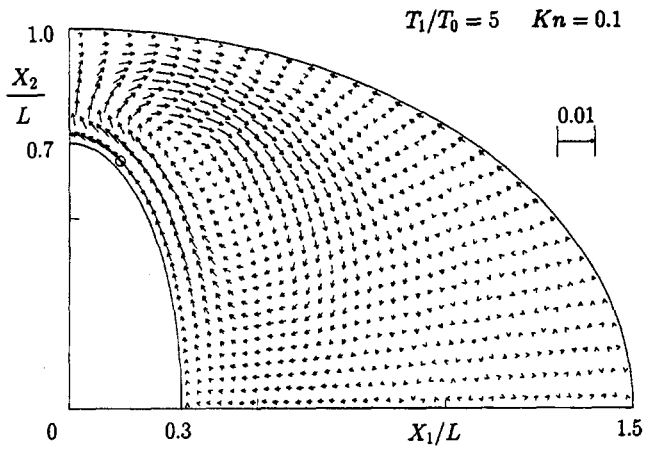

(a)

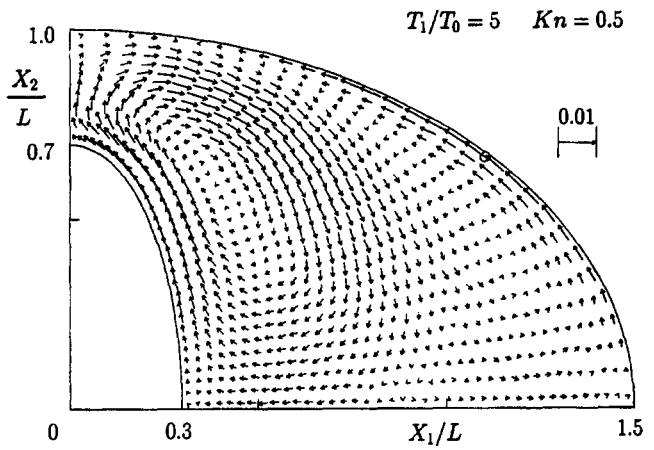

(b)

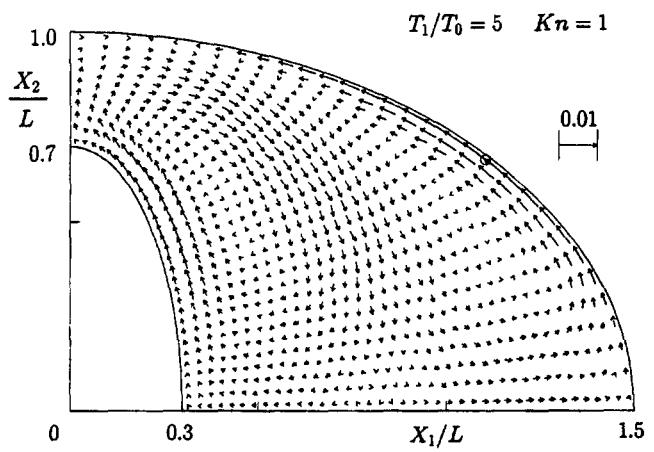

(c)

Figure 2. Flow-velocity field for $a_0 = 0.3$, $b_0 = 0.7$, and $a_1 = 1.5$ and for $T_1/T_0 = 5$. (a) Kn = 0.1, (b) Kn = 0.5, (c) Kn = 1, (d) Kn = 2, (e) Kn = 5. The arrows indicate the nondimensional flow velocity $\mathbf{v}/(2RT_0)^{1/2}(v_3 = 0)$ at their starting points, and their scale is shown in the figures. The symbol ○ represents the point with the maximum speed, and the values $|\mathbf{v}|_{\max}/(2RT_0)^{1/2}$ are 5.72×10^{-3} (Kn = 0.1), 6.58×10^{-3} (Kn = 0.5), 7.30×10^{-3} (Kn = 1), 5.72×10^{-3} (Kn = 2), and 3.69×10^{-3} (Kn = 5).

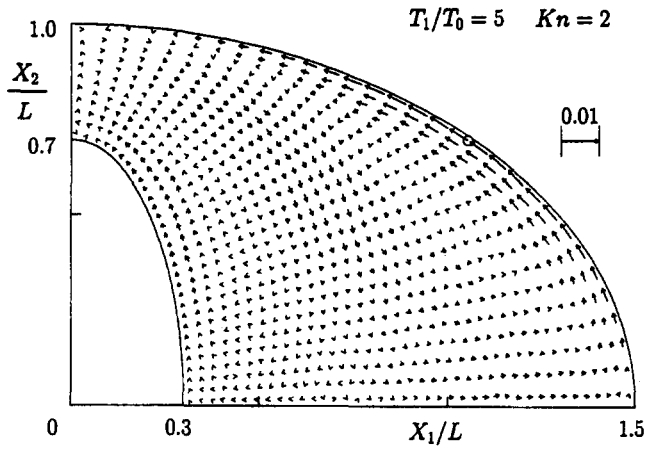

(d)

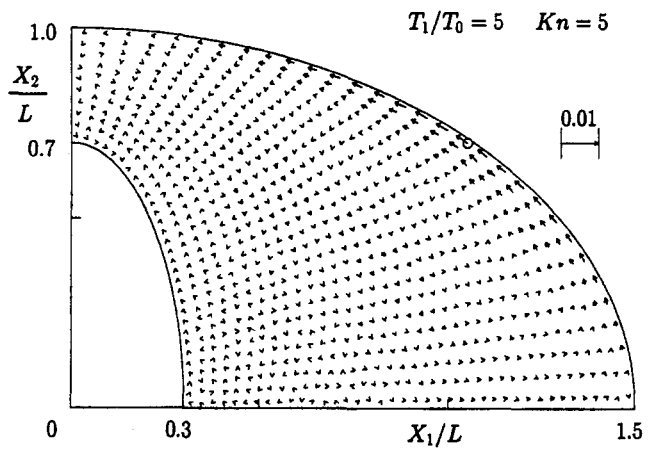

(e)

Figure 2. (cont.)

Figure 2, the flow-velocity field (in the first quadrant) is shown for Kn = 0.1, 0.5, 1, 2, and 5, where the arrows indicate the nondimensional flow velocity $\mathbf{v}/(2RT_0)^{1/2}$ with $v_3 = 0$ at their starting points and their scale is shown in each figure. The symbol ○ in Figure 2 indicates the point with the maximum speed $|\mathbf{v}|_{\max}/(2RT_0)^{1/2}$, the magnitude of which is given in the caption. Figure 3 shows the isothermal and isodensity lines for Kn = 0.1, 0.5, 2, and ∞. At Kn = 0.1, a clockwise circulating flow is induced along the inner cylinder and is dominant in the flow field. But, if we observe carefully, we notice that a slow counterclockwise circulating flow is also induced along the outer cylinder. At Kn = 0.5, the flow speed increases on the whole; in particular, the flow along the outer cylinder is intensified significantly. As Kn is increased to 1, the inner clockwise flow weakens considerably, whereas the outer counterclockwise flow still grows slightly. With the further increase of Kn (Kn = 1 → 2 → 5), the inner flow attenuates rapidly, but the decay of the outer flow is slow. The flow vanishes in the free molecular case (Kn = ∞). This fact is proved rigorously in a more general system (arbitrary shapes, arrangement, and temperature distributions of the vessel and bodies and Maxwell-type boundary condition) in [20,21], where the exact solution describing the general behavior of a free molecular gas in a closed domain (or an open domain with certain conditions at infinity) with boundaries of arbitrary shapes and temperature distributions is constructed. The temperature and density fields in Figure 3d are the result of this exact solution. The behavior of the gas for small Kn is described by the asymptotic theory in [4]. According to it, the flow vanishes in the continuum limit Kn→ 0, but, contrary to the general understanding, the temperature field in this limit is different from that obtained

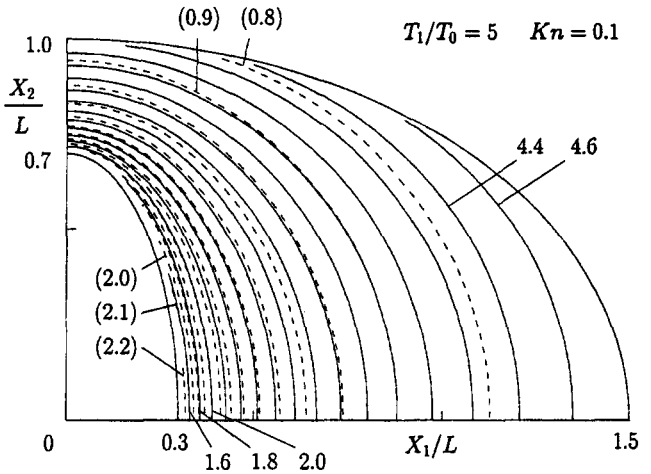

(a)

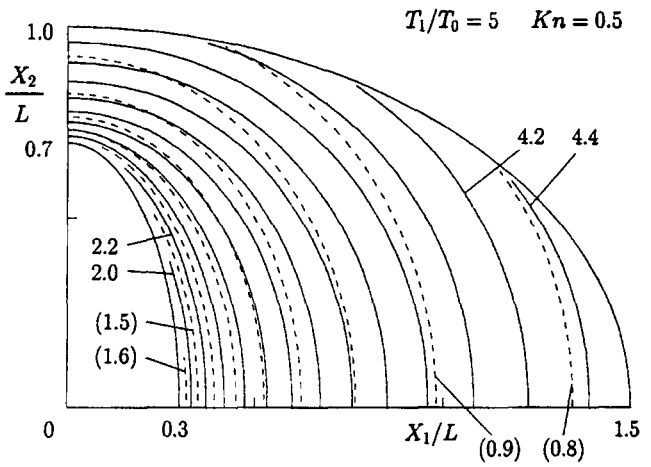

(b)

Figure 3. Isothermal and isodensity lines for $a_0 = 0.3$, $b_0 = 0.7$, and $a_1 = 1.5$ and for $T_1/T_0 = 5$. (a) Kn = 0.1, (b) Kn = 0.5, (c) Kn = 2, (d) Kn = ∞. The line — indicates the isothermal lines: $T/T_0 = 1.6 + 0.2m$, $m = 0, 1, \ldots, 15$ in (a); $T/T_0 = 2.0+0.2m$, $m = 0, 1, \ldots, 12$ in (b); $T/T_0 = 2.2+0.2m$, $m = 0, 1, \ldots, 10$ in (c); and $T/T_0 = 2.4+0.1m$, $m = 0, 1, \ldots, 15$ in (d). The line - - - - indicates the isodensity lines: $\rho/\rho_0 = 2.2 - 0.1m$, $m = 0, 1, \ldots, 14$ in (a); $\rho/\rho_0 = 1.6 - 0.1m$, $m = 0, 1, \ldots, 8$ in (b); $\rho/\rho_0 = 1.35 - 0.05m$, $m = 0, 1, \ldots, 10$ in (c); and $\rho/\rho_0 = 1.2 - 0.025m$, $m = 0, 1, \ldots, 11$ in (d).

by the heat-conduction equation (the correct system of the equations and boundary conditions is given in [4]). For small Kn, the local properties of the system determine the flow field; various flows such as the thermal stress slip flow [2,9,10] and the nonlinear thermal stress flow [4,5,11] are induced in this situation. In order to describe the above behavior of the gas by the Boltzmann equation (without the help of the asymptotic theory), a very accurate numerical analysis for small Kn is required, which is a difficult task, as is seen from [4]. In particular, the DSMC computation with such high accuracy is practically impossible.

To see the effects of the temperature ratio and geometry, two typical examples are shown in Figures 4 and 5. The flow-velocity field and the isothermal and isodensity lines in the case with the same geometry ($a_0 = 0.3$, $b_0 = 0.7$, and $a_1 = 1.5$) but with a smaller temperature ratio $T_1/T_0 = 2$ are shown for Kn = 0.5 in Figure 4. The features of the flow pattern are more or less the same as Figure 2b, but the flow speed is reduced considerably. The corresponding results in the system where the inner cylinder is a circular cylinder of radius $0.6L$ (i.e., $a_0 = b_0 = 0.6$

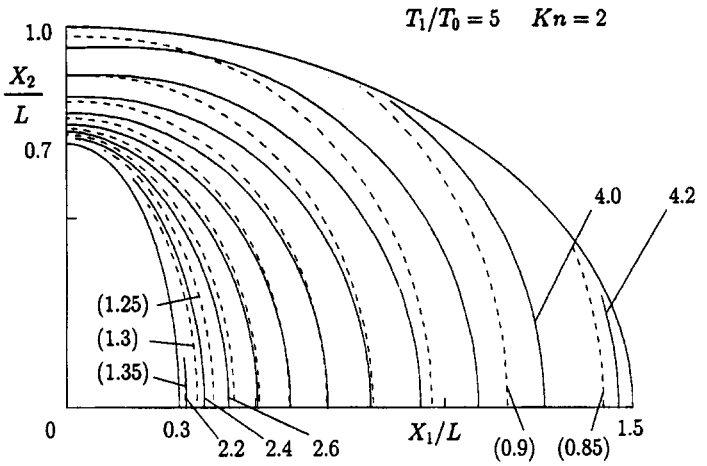

(c)

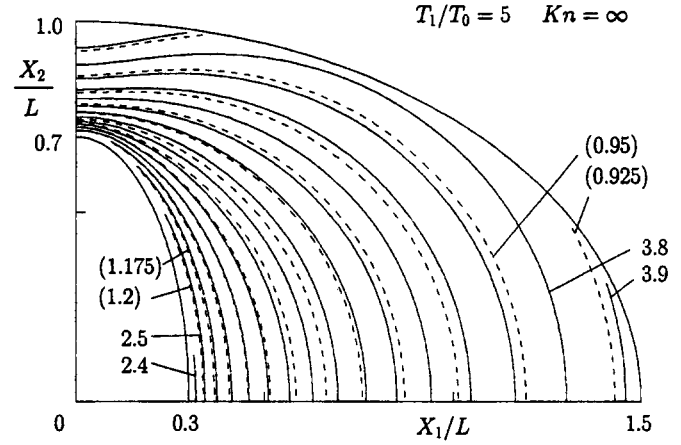

(d)

Figure 3. (cont.)

and $a_1 = 1.5$) are shown for $T_1/T_0 = 5$ and Kn $= 0.5$ in Figure 5. It is seen from Figures 2b and 5a that the flow pattern is quite different depending on the shape of the inner cylinder. In Figure 5a, the inner clockwise flow disappears and the outer counterclockwise flow extends to the inner cylinder.

The data on the simulation scheme used to obtain the results in Figures 2–5 (except Figure 3d which is based on the exact solution) are summarized as follows.

(a) *Initial condition*: The Maxwellian distribution with density ρ_0, temperature T_0, and flow velocity zero is taken as the initial velocity distribution $f^{(0)}$.

(b) *Cells*: The system of simulation cells used in the computation for Figures 2–4 ($a_0 = 0.3$, $b_0 = 0.7$, and $a_1 = 1.5$) is shown in Figure 6. Here, the gas region (in the first quadrant) is first divided into fine sub-cells by the lines $X_1/L = na_1/600$ ($a_1 = 1.5$, $n = 1, 2, \ldots, 599$) and $X_2/L = n'/400$ ($n' = 1, 2, \ldots, 399$) (thus, each sub-cell is the square with side length $L/400$, except irregular ones in contact with the cylinder surfaces). The simulation cells are then formed in such a way that each cell is a cluster of a number of sub-cells. The total number of simulation cells is 775. In the case of Figure 5 ($a_0 = b_0 = 0.6, a_1 = 1.5$), a different system of cells (546 cells), constructed in a similar way, was used.

(c) *Particles*: The total number of particles N is 775000 for Figures 2–4 and 546000 for Figure 5.

(d) *Time step*: The time step Δt is $5t_0/10^2\sqrt{\pi}$ for Kn $= 0.1$ and $t_0/10^2\sqrt{\pi}$Kn for Kn ≥ 0.5, where t_0 is the mean free time corresponding to l_0, i.e., $t_0 = (\sqrt{\pi}/2)(2RT_0)^{-1/2}l_0$.

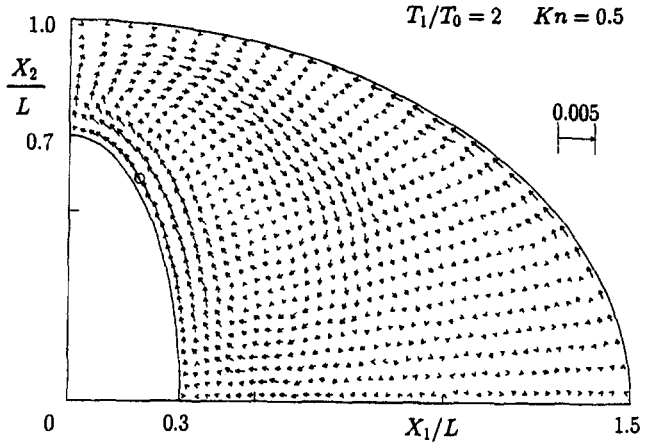

(a) Flow-velocity field.

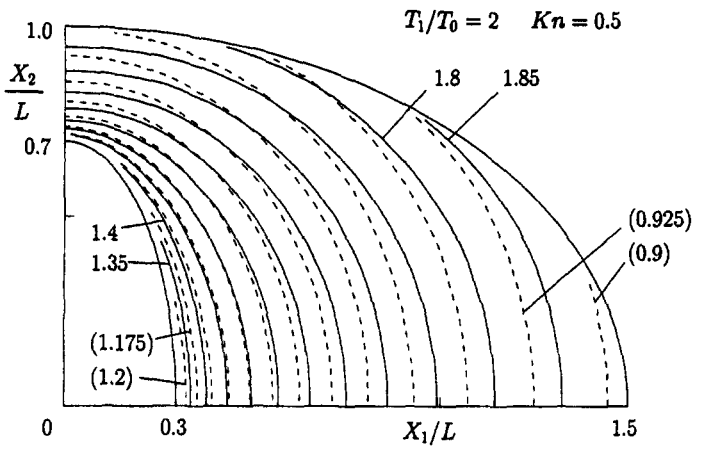

(b) Isothermal and isodensity lines.

Figure 4. Flow-velocity field and isothermal and isodensity lines at Kn = 0.5 for a *smaller temperature ratio* $T_1/T_0 = 2$ and for $a_0 = 0.3$, $b_0 = 0.7$, and $a_1 = 1.5$ (the same geometry as Figure 2). In (a), the arrows indicate the nondimensional flow velocity $\mathbf{v}/(2RT_0)^{1/2}$ ($v_3 = 0$) at their starting points, and their scale is shown in the figure; the symbol ○ represents the point with the maximum speed, where $|\mathbf{v}|_{\max}/(2RT_0)^{1/2} = 2.44 \times 10^{-3}$. In (b), — indicates the isothermal lines $T/T_0 = 1.35 + 0.05m$, $m = 0, 1, \ldots, 10$, and ---- the isodensity lines $\rho/\rho_0 = 1.2 - 0.025m$, $m = 0, 1, \ldots, 12$.

(e) *Collision process*: In the step (iv) of Section 4, $M_{(\ell)}$ is assumed to be $0.3N_{(\ell)}$ for Kn = 0.1 and $0.1N_{(\ell)}$ for Kn $\geq$ 0.5 in all the cells and all the time.

(f) *Average*: In Figures 2–5, the averages of the data at each two time steps over the interval $2 \times 10^5 \Delta t$ are shown for Kn = 0.1, and those of the data at each time step over $10^5 \Delta t$ are shown for Kn $\geq$ 0.5. The averages are taken after the steady state is judged to be established.

In addition to the above data, we make some supplementary remarks related to the computation. First, the system of cells in (b), where the cell sides except ones on the boundary are parallel to the X_1 or X_2 axis though zigzag, is convenient for determining in which cell the particles lie after step (iii) in Section 4, and thus allows a highly efficient computation. Secondly, we monitored the probability $P_{M(\ell)}^{(j,k)}$ (equation (13)) in the step (iv) of Section 4 for the choice of $M_{(\ell)}$ in (e) because it should be less than 1. In the test for $a_0 = 0.3$, $b_0 = 0.7$, and $a_1 = 1.5$ and for $T_1/T_0 = 5$ over 6000 time steps with 77500 particles for Kn = 0.5, 1 and with 775000 particles for Kn = 0.1, the observed maximum of $P_{M(\ell)}^{(j,k)}$ is 0.6447 (Kn = 0.1), 0.6701 (Kn = 0.5),

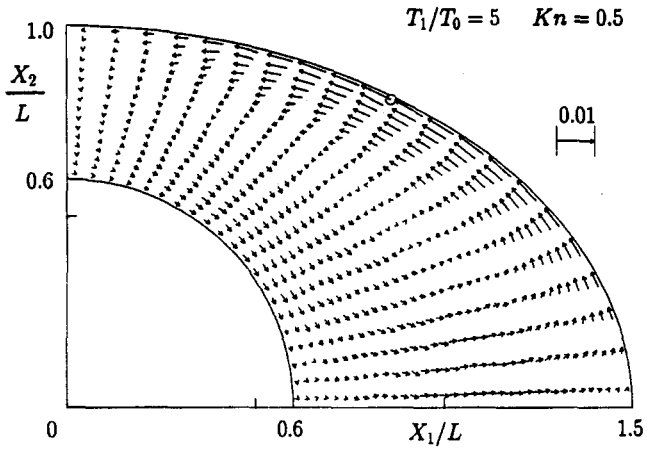

(a) Flow-velocity field.

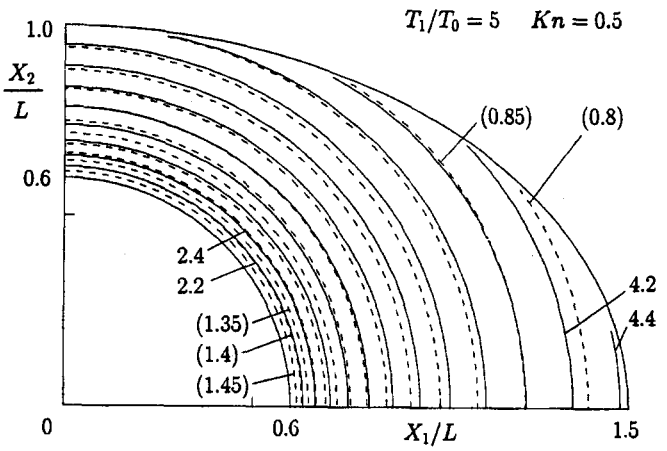

(b) Isothermal and isodensity lines.

Figure 5. Flow-velocity field and isothermal and isodensity lines at Kn = 0.5 for $T_1/T_0 = 5$ when *the inner cylinder is a circular one*, i.e., $a_0 = b_0 = 0.6$, $a_1 = 1.5$. In (a), the arrows indicate the nondimensional flow velocity $\mathbf{v}/(2RT_0)^{1/2}(v_3 = 0)$ at their starting points, and their scale is shown in the figure; the symbol ○ represents the point with the maximum speed, where $|\mathbf{v}|_{\max}/(2RT_0)^{1/2} = 8.64 \times 10^{-3}$. In (b), — indicates the isothermal lines $T/T_0 = 2.2 + 0.2m$, $m = 0, 1, \ldots, 11$, and ---- the isodensity lines $\rho/\rho_0 = 1.45 - 0.05m$, $m = 0, 1, \ldots, 13$.

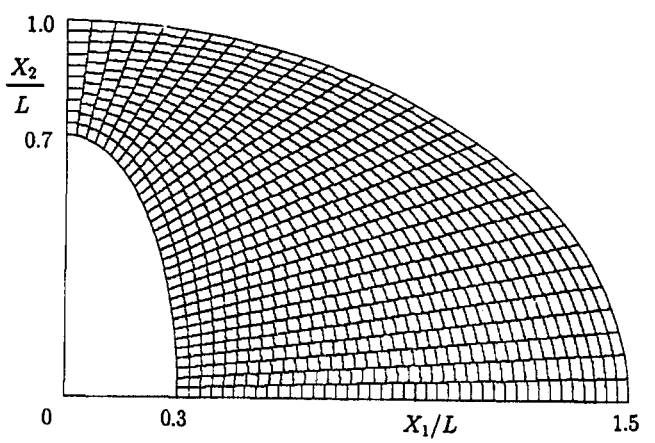

Figure 6. System of cells used for $a_0 = 0.3$, $b_0 = 0.7$, and $a_1 = 1.5$.

and 0.3735 (Kn = 1). Further, in the same test with $M_{(\ell)} = 0.1N_{(\ell)}$ and $M_{(\ell)} = 0.2N_{(\ell)}$ for Kn = 0.1, the $P_{M(\ell)}^{(j,k)}$ exceeds 1 for 0.0134 percent of all the pairs chosen for the check of collision when $M_{(\ell)} = 0.1N_{(\ell)}$ ($\max P_{M(\ell)}^{(j,k)} = 1.8516$), and only for 2.2×10^{-8} percent (only two pairs) when $M_{(\ell)} = 0.2N_{(\ell)}$ ($\max P_{M(\ell)}^{(j,k)} = 1.0218$). Thirdly, the X_3 component v_3 of the flow velocity, which should be zero exactly, does not vanish in the actual computation because of the limitations of computational condition (finite particle number, finite cell size, etc.). This gives a measure of accuracy of the computation. In our computation, $|v_3|/(2RT_0)^{1/2}$ is less than 4.70×10^{-4}, 4.59×10^{-4}, 4.22×10^{-4}, 4.95×10^{-4}, 4.72×10^{-4}, 3.58×10^{-4}, and 4.45×10^{-4}, respectively, in the case of Figures 2a, 2b, 2c, 2d, 2e, 4, and 5 in 80% of the cells in the domain (the maximum flow speed in the X_1X_2 plane, $(v_1^2 + v_2^2)_{\max}^{1/2}/(2RT_0)^{1/2}$, in each case is given in the captions of Figures 2, 4, and 5). Finally, we also carried out the computation corresponding to Figure 2 with a smaller number of particles (77500 particles). Its flow velocity, the fluctuation of which is larger than that in Figure 2, agrees well with Figure 2, and its isothermal and isodensity lines agree completely with those obtained by using 775000 particles (e.g., Figures 3a–3c).

The computation was carried out on HP9000 735 workstations in the Fluid Dynamics Laboratory, Department of Aeronautics and Astronautics, Graduate School of Engineering, Kyoto University.

6. DISCUSSIONS

Referring to the results in Figures 2 and 3, we briefly discuss the physical mechanism of the flow. In the following, we assume $T_0 < T_1$ as in Figures 2 and 3.

To begin with, we consider the flow along the inner cylinder. For small Kn, the velocity distribution of the gas molecules is determined by the local properties of the macroscopic variables, i.e., ρ, $\mathbf{v}$, T and their derivatives. The state of the gas near the inner cylinder in Figures 2a and 3a, where Kn = 0.1, seems to be fairly close to this situation because the local density ρ is about $2\rho_0$ and thus the local mean free path is about $l_0/2$ there. The temperature field in Figure 3a shows that the temperature gradient in the gas near the inner cylinder has not only the component normal to the cylinder surface but also the component parallel (or tangential) to it. Owing to this tangential temperature gradient, a flow is induced along the cylinder from the colder part to the hotter part by the same mechanism as the thermal creep flow [6–8,13], in spite of the fact that the temperature of the cylinder itself is uniform. On the other hand, for moderate and large Kn, the velocity distribution of the gas molecules is not characterized by the local properties of the macroscopic variables but is affected by the overall properties of the system, such as its configuration. In the free molecular flow (Kn = ∞), where the gas flow vanishes, the velocity distribution of the molecules impinging on the inner cylinder is isotropic. This fact is not obvious but the consequence of [20,21]. Since the velocity distribution of the outgoing molecules is isotropic in the case of the diffuse reflection, no tangential force acts on the surface of the cylinder. When Kn is large but finite, the isotropy of the velocity distribution of the impinging molecules is distorted by molecular collisions because the configuration is not symmetric. This gives a tangential force on the cylinder. The reaction of this force, which is imparted to the gas by molecular collisions, induces a flow. For large Kn, the distortion of isotropy of the velocity distribution of the impinging molecules is small, and, in addition, molecular collisions that transfer the reaction to the gas near the cylinder are rare. Therefore, the induced flow vanishes rapidly as Kn is increased. The mechanism described above is essentially the same as that given in [17], where a flow induced along a flat plate (instead of an elliptic cylinder) is investigated. The striking difference is that, in the case of the flat plate, a very steep temperature gradient in the direction parallel to the plate arises in the gas along the plate near the edges, and thus a localized but intense flow is induced there.

We next consider the flow induced along the outer cylinder. This flow is caused by a different mechanism clarified in [16], where a gas flow induced between two noncoaxial circular cylinders

with slightly different temperatures is studied by an accurate finite-difference analysis of the linearized BKW equation. We will outline the mechanism in a slightly different way. As we have mentioned, no flow is induced in the free molecular case (Kn = ∞). Now let us look at a point (say, point A) on the outer cylinder where the tangential velocity is appreciable in Figure 2b, 2c, or 2d, and let us consider the mass flux due to the molecules impinging on point A from a given direction. According to the general theory [20,21], the flux does not depend on the direction in the free molecular flow (Kn = ∞). Molecular collisions affect the flux. The gas in the upper left region in Figure 2 is more cooled by the inner cylinder than that in the lower right region (see Figure 3). The molecules impinging on point A from the upper left region are more cooled or decelerated by molecular collisions in the cooler region. Therefore, the total mass flux due to the molecules impinging on point A is in the upper leftward direction. Since the velocity distribution of the outgoing molecules is isotropic, a flow occurs in the upper leftward direction along the outer cylinder. As Kn is decreased, the effect of molecular collisions becomes larger, and thus the flow is intensified. At sufficiently small Kn, where the state of the gas is characterized by local properties of the macroscopic variables, the mechanism described above does not apply, and other types of flow, such as the thermal creep flow, thermal stress slip flow, and nonlinear thermal stress flow, become important. The mechanism outlined above should not be confused with that of the thermal creep flow. In the latter, a stationary state with a temperature gradient along the boundary is first considered, where the mass fluxes of the impinging molecules from the two directions are balanced and therefore the momentum flux to a small surface element is estimated to have a tangential component, and the momentum exchange between the gas and the boundary wall is discussed. The molecules reflected on the wall soon collide with another molecule and establish a flow near the wall in such a way that the tangential momentum flux of the impinging molecules is canceled. In the former, on the other hand, the reflected molecules proceed some distance without collision and thus do not cause their direct effect on the gas near point A; the molecules coming from the neighboring wall retain their property. Thus the global configuration is important. (The free molecular flow is its extreme case.)

The entire flow field is determined by the balance of the two types of flow at each Kn. In Figure 5a, where the inner cylinder is a circular one, the flow along the outer cylinder does not show a large difference from that in Figure 2b, as expected from the mechanism of the flow. On the other hand, Figure 5b shows that the density and temperature fields in the gas are almost cylindrically symmetric. This means that the velocity distribution of the molecules impinging on the circular cylinder is almost isotropic. Therefore, the upward flow along the inner cylinder (cf. Figure 2b) disappears, and the circulating flow driven on the outer cylinder extends to the inner cylinder.

REFERENCES

1. Y. Sone, Asymptotic theory of flow of rarefied gas over a smooth boundary I, In *Rarefied Gas Dynamics*, (Edited by L. Trilling and H.Y. Wachman), Vol. 1, pp. 243–253, Academic Press, New York (1969).
2. Y. Sone, Asymptotic theory of flow of rarefied gas over a smooth boundary II, In *Rarefied Gas Dynamics*, (Edited by D. Dini), Vol. 2, pp. 737–749, Editrice Tecnico Scientifica, Pisa (1971).
3. Y. Sone, Asymptotic theory of a steady flow of a rarefied gas past bodies for small Knudsen numbers, In *Advances in Kinetic Theory and Continuum Mechanics*, (Edited by R. Gatignol and Soubbaramayer), pp. 19–31, Springer-Verlag, Berlin (1991).
4. Y. Sone, K. Aoki, S. Takata, H. Sugimoto and A.V. Bobylev, Inappropriateness of the heat-conduction equation for description of a temperature field of a stationary gas in the continuum limit: Examination by asymptotic analysis and numerical computation of the Boltzmann equation, *Phys. Fluids* **8** (2), 628–638 (1996).
5. Y. Sone and K. Aoki, *Molecular Gas Dynamics*, (in Japanese), Asakura, Tokyo, (1994).
6. E.H. Kennard, *Kinetic Theory of Gases*, McGraw-Hill, New York, (1938).
7. Y. Sone, Thermal creep in rarefied gas, *J. Phys. Soc. Jpn.* **21** (9), 1836–1837 (1966).
8. T. Ohwada, Y. Sone and K. Aoki, Numerical analysis of the shear and thermal creep flows of a rarefied gas over a plane wall on the basis of the linearized Boltzmann equation for hard-sphere molecules, *Phys. Fluids A* **1** (9), 1588–1599 (1989).

9. Y. Sone, Flow induced by thermal stress in rarefied gas, *Phys. Fluids* **15** (8), 1418–1423 (1972).
10. T. Ohwada and Y. Sone, Analysis of thermal stress slip flow and negative thermophoresis using the Boltzmann equation for hard-sphere molecules, *Eur. J. Mech., B/Fluids* **11** (4), 389–414 (1992).
11. M.N. Kogan, V.S. Galkin and O.G. Fridlender, Stresses produced in gases by temperature and concentration inhomogeneities. New type of free convection, *Sov. Phys. Usp.* **19** (5), 420–438 (1976).
12. T. Ohwada, Y. Sone and K. Aoki, Numerical analysis of the Poiseuille and thermal transpiration flows between two parallel plates on the basis of the Boltzmann equation for hard-sphere molecules, *Phys. Fluids A* **1** (12), 2042–2049 (1989); Erratum: *Phys. Fluids A* **2** (4), 639 (1990).
13. S. Takata and Y. Sone, Flow induced around a sphere with a nonuniform surface temperature in a rarefied gas, with application to the drag and thermal force problems of a spherical particle with an arbitrary thermal conductivity, *Eur. J. Mech., B/Fluids* **14** (4), 487–518 (1995).
14. G.A. Bird, *Molecular Gas Dynamics*, Oxford University Press, Oxford, (1976).
15. G.A. Bird, *Molecular Gas Dynamics and the Direct Simulation of Gas Flows*, Oxford University Press, Oxford, (1994).
16. K. Aoki, Y. Sone and T. Yano, Numerical analysis of a flow induced in a rarefied gas between noncoaxial circular cylinders with different temperatures for the entire range of the Knudsen number, *Phys. Fluids A* **1** (2), 409–419 (1989).
17. K. Aoki, Y. Sone and N. Masukawa, A rarefied gas flow induced by a temperature field, In *Rarefied Gas Dynamics*, (Edited by J. Harvey and G. Lord), Vol. 1, pp. 35–41, Oxford University Press, Oxford (1995).
18. C. Cercignani, *The Boltzmann Equation and Its Applications*, Springer-Verlag, Berlin, (1988).
19. W. Wagner, A convergence proof for Bird's direct simulation Monte Carlo method for the Boltzmann equation, *J. Stat. Phys.* **66** (3/4), 1011–1044 (1992).
20. Y. Sone, Highly rarefied gas around a group of bodies with various temperature distributions. I. Small temperature variation, *Journal de Mécanique Théorique et Appliquée* **3** (2), 315–328 (1984).
21. Y. Sone, Highly rarefied gas around a group of bodies with various temperature distributions. II. Arbitrary temperature variation, *Journal de Mécanique Théorique et Appliquée* **4** (1), 1–14 (1985).